Macromolecules

ARTICLE

pubs.acs.org/Macromolecules

Structure and Mechanism of Strength Enhancement in Interpenetrating Polymer Network Hydrogels

Dale J. Waters,[†] Kristin Engberg,[†] Rachel Parke-Houben,[†] Christopher N. Ta,[‡] Andrew J. Jackson,[§,∥] Michael F. Toney,[⊥] and Curtis W. Frank*[,†]

[†]Department of Chemical Engineering, Stanford University, 381 North-South Mall, Stauffer III, Stanford, California 94305-5025, United States

[‡]Department of Ophthalmology, Stanford University School of Medicine, 300 Pasteur Drive Stanford, California 94305-5025, United States

[§]NIST Center for Neutron Research, National Institute of Standards and Technology,100 Bureau Drive, Gaithersburg, Maryland 20899-6102, United States

[∥]Department of Chemical Engineering, University of Delaware, 150 Academy Street, Newark, Delaware 19716, United States

[⊥]Stanford Synchrotron Radiation Lightsource, Menlo Park, California 94025-7015, United States

Supporting Information

ABSTRACT: Hydrogels with high modulus and fracture strength are obtained by interpenetrating a tightly cross-linked poly(ethylene glycol) (PEG) network with a loosely cross-linked poly(acrylic acid) (PAA) network. Small-angle X-ray and neutron scattering (SAXS/SANS) are used in conjunction with swelling measurements to determine the structure of PEG/PAA interpenetrating polymer networks (IPNs) and to measure the average PEG chain extension within the IPN. At pH 7.4, the PEG chains within the IPN are extended to 45−70% of their maximum achievable length as a result of expansion of the ionized PAA network within the IPN. Near these high extension ratios, the force required to further strain the PEG chains is increased due to the entropic effects of finite chain extensibility. This leads to PEG/PAA IPN hydrogels with a 3-fold increase in both compressive modulus and fracture strength compared to PEG single networks with the same polymer volume fraction. The structure, mechanical properties, and mechanisms of strength enhancement for PEG/PAA IPN hydrogels are notably different than for the high toughness double-network hydrogels previously described by Gong et al.

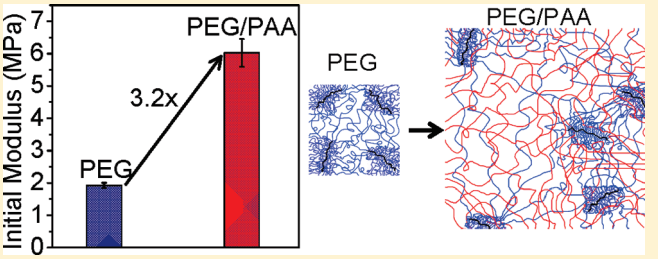

INTRODUCTION

Hydrogels are networks of hydrophilic polymers that are insoluble in water due to network cross-links. Hydrogels are attractive materials for replacement of natural soft tissues and as three-dimensional cell scaffolds because they can swell to high water content (>80 wt %), mimicking that of natural tissue. The high water content of hydrogels is often a critical attribute because it allows for a high rate of cell nutrient and waste product diffusion through the material. However, a critical disadvantage for most high-water-content hydrogels is that they are generally fragile materials with low modulus and/or fracture strength. The typically inadequate mechanical properties of hydrogels restrict their use to applications that require little or no mechanical strength.

In recent years, there have been a number of efforts to generate hydrogels with both high water content and improved mechanical properties. Perhaps most notably, Gong and co-workers have developed a class of high-tear-strength hydrogels based on interpenetrating polymer networks (IPNs).[1] These IPN hydrogels are referred to as "double-network" hydrogels and consist of a tightly cross-linked ionized poly(2-acrylamido-2-methylpropanesulfonic acid) (PAMPS) first network and a loosely cross-linked neutral polyacrylamide (PAAm) second network. The mechanical properties and the mechanisms of strength enhancement in these hydrogels have been studied extensively in recent years.[1−15] Briefly, Gong's proposed mechanism of tear strength enhancement involves the loosely cross-linked second network, which is ductile, holding together fractures that occur in the tightly cross-linked first network, which is brittle. This tear force dissipation mechanism confines the tear damage zone to a small area surrounding the crack tip rather than allowing the crack to propagate throughout the hydrogel.

Inspired by the work of Gong and co-workers, Myung and co-workers have developed a related IPN hydrogel system for an artificial cornea application wherein the order of the ionized and neutral networks within the IPN is inverted.[16,17] In this system,

Received: March 25, 2011
Revised: June 14, 2011
Published: June 27, 2011

tightly cross-linked neutral poly(ethylene glycol) (PEG) is used as the first network and loosely cross-linked ionized poly(acrylic acid) (PAA) is used as the second network. Although a dramatic strength enhancement is also observed in these hydrogels, the principal mechanical property enhanced is the elastic modulus rather than the tear strength. Accordingly, the molecular-level structure and the mechanisms of strength enhancement for PEG/PAA IPN hydrogels are quite different from the PAMPS/PAAm IPN hydrogels. Here, we elucidate the differences between these two IPN hydrogel systems by investigating the structure and the mechanisms of strength enhancement for PEG/PAA IPN hydrogels using a combination of swelling, small-angle X-ray scattering (SAXS), small-angle neutron scattering (SANS), and compressive mechanical testing techniques.

In previous work, we used SAXS to study the morphology of photopolymerized end-linked PEG-diacrylate and PEG-diacrylamide hydrogels that serve as the first network in the PEG/PAA IPN system.[18] This work established that these PEG hydrogels have short-range ordering, as indicated by a correlation peak in the SAXS pattern. This correlation peak was determined to be related to the spacing between high functionality cross-link junctions within the PEG network. In the present study, we use swelling measurements along with SAXS/SANS to investigate what happens to the molecular-level structure of these PEG networks when they are interpenetrated with a loosely cross-linked PAA network, which exhibits extensive swelling when ionized at physiological pH 7.4. The swelling properties and the structural changes are evaluated as a function of pH and are related to the enhancement in modulus that occurs during the transition from a PEG single network to a PEG/PAA IPN at pH 7.4. The strength enhancement mechanism described in this work may provide a general method to enhance the modulus and fracture strength of swollen polymer networks without increasing the polymer content.

EXPERIMENTAL SECTION

Chemicals. 2-Hydroxy-2-methylpropiophenone, acrylic acid, acryloyl chloride, diol-terminated poly(ethylene glycol) (PEG) [M_n = 3400 g/mol (prod. # 202444), M_n = 4600 mol (prod. # 373001), M_n = 8000 g/mol (prod. # 202452)], triethylamine, and triethylene glycol dimethacrylate were purchased from Sigma-Aldrich Chemical Co. (Milwaukee, WI) and used as received. Dichloromethane, diethyl ether, and anhydrous tetrahydrofuran were purchased from Fisher Scientific (Pittsburgh, PA). Deuterated acrylic acid was obtained from CDN Isotopes Inc. (Pointe-Claire, Quebec).

PEG-Diacrylate Synthesis. Diacrylate-terminated PEG macromonomers were prepared by reacting diol-terminated PEG with a 2.5 molar excess of acryloyl chloride and triethylamine base catalyst in tetrahydrofuran overnight at room temperature, as described previously.[18,19] It should be noted that the previous work by Myung and co-workers followed a different PEG-diacrylate synthesis procedure, which did not use triethylamine as a base catalyst and used a less extensive purification protocol compared to the current work.[16] PEG-diacrylate was prepared with three different PEG molecular weights (M_n = 3400 g/mol, M_n = 4600 g/mol, and M_n = 8000 g/mol). From here on, PEG-diacrylate will be denoted as PEG(M_n), where the number-average molecular weight, M_n, when specified, is abbreviated as 3.4K for M_n = 3400 g/mol, 4.6K for M_n = 4600 g/mol, and 8.0K for M_n = 8000 g/mol.

PEG/PAA IPN Hydrogel Synthesis. PEG/PAA IPN hydrogels were prepared via sequential two-step free-radical photopolymerization. To prepare the first network, dried PEG-diacrylate powder was dissolved in deionized water at a concentration of 50% w/w. The photoinitiator, 2-hydroxy-2-methyl-propiophenone, was then added to the solution at 1 wt % with respect to the PEG macromonomer. PEG macromonomer solutions with photoinitiator were injected between two glass slides separated by a Teflon spacer to control the hydrogel thickness. The PEG precursor solutions were then exposed to an ultraviolet (UV) light source (365 nm at 10 mW/cm^2) for 5 min (UV chamber model ELC-500, Electro-lite Corporation, Danbury, CT). Upon exposure to UV light, the macromonomer end-groups reacted via free radical photopolymerization to create an end-linked PEG network.

To incorporate the PAA second network, the PEG hydrogel was soaked overnight in an excess volume (120 mL of solution per gram of PEG macromonomer) of a 50% v/v (7.3 M) acrylic acid/deionized water solution (pH 1.7) with 1 vol % (0.45 mol %) 2-hydroxy-2-methylpropiophenone photoinitiator and 1 vol % (0.26 mol %) triethylene glycol dimethacrylate cross-linker. After the PEG hydrogel had soaked overnight in the acrylic acid solution and had reached its equilibrium swelling point, the acrylic acid-soaked PEG hydrogel was placed back between glass slides and exposed to the same UV light source for 5 min. Upon exposure to UV light, a loosely cross-linked PAA network was generated in the presence of the first PEG network, which resulted in an IPN structure.

To remove any unreacted monomers and to equilibrate the hydrogels to the desired pH, the PEG/PAA IPN hydrogels were washed extensively in a continuously stirred 1 L tank with an inlet of pH buffered solution at a rate of 5 L/day. This washing procedure allowed the pH of the PEG/PAA IPN hydrogels to gradually rise from the pH of the acrylic acid soaking solution (pH 1.7) to the desired pH of the buffer. The washing process took ~3 days, depending on the thickness of the hydrogel.

Swelling Measurements. To determine the amount of PEG and PAA polymer incorporated into the IPN hydrogels, the masses of 12 mm diameter hydrogel discs were recorded for both fully swollen and fully dried hydrogels after each step in the IPN hydrogel synthesis protocol. Swelling measurements were made in triplicate. Mass fractions of PEG and PAA were obtained and converted to volume fractions using a specific volume of 0.92 cm^3/g for PEG and a specific volume of 0.82 cm^3/g for PAA.[20] Error bars for swelling measurements represent one standard deviation in the data.

Since PAA is a pH-sensitive polymer with pK_a ≈ 4.3, swelling measurements for PEG/PAA IPNs were studied as a function of pH.[21] PEG/PAA IPNs were swollen in 13 different buffer solutions ranging from pH 3.0 (carboxylic acid groups on PAA are nearly completely protonated) to pH 7.4 (physiologically relevant pH for which carboxylic acid groups on PAA are nearly completely deprotonated). The pH values of the buffer solutions were incremented by 0.5 pH units at pH values far from the pK_a of PAA and by 0.25 pH units at pH values near the pK_a of PAA. A potassium hydrogen phthalate buffer was used for the pH values 3.0, 3.5, 3.75, 4.0, 4.25, 4.5, 4.75, 5.0, and 5.5, while a phosphate buffer was used for the pH values 6.0, 6.5, 7.0, and 7.4. Ionic strength was kept constant at 0.15 M using sodium chloride for all buffers.

Small-Angle X-ray Scattering (SAXS) Measurements. SAXS measurements were performed at the Stanford Synchrotron Radiation Lightsource (SSRL) on beamlines 1-4 and 4-2. Hydrogel samples between 0.5 and 1.0 mm thick and 15 mm diameter were placed into sample holders with no windows. Sample measurement times were 10 min on bending magnet beamline 1-4 or 1 min on the more intense wiggler beamline 4-2. Over this time frame, no noticeable dehydration of the hydrogel samples occurred. Background and empty cell scattering signals were determined in separate measurements with no beam and empty sample holders, respectively. Depending upon the sample-to-detector distance, this distance and the beam centers were calibrated with silver behenate, cholesteryl myristate, or chicken collagen standard samples. Multiple sample-to-detector distances were used, and the

overlapping data were aligned by shifting intensities by an arbitrary factor. The uncertainty in the measured SAXS intensity is less than the size of the plotting symbols. All fitting of scattering curves was performed using a Levenberg−Marquardt nonlinear regression algorithm within OriginPro8 software (OriginLab, Northampton, MA).

Small-Angle Neutron Scattering (SANS) Measurements. SANS measurements were performed on the 30 m NG-7 beamline at the NIST Center for Neutron Research (NCNR) located at the National Institute for Standards and Technology (NIST) in Gaithersburg, MD. Hydrogel samples roughly 2 mm thick were placed into 2 mm thick sample holders with quartz windows. An excess of buffer solution was added to the sample holders before they were sealed to keep the hydrogels hydrated during the course of the SANS measurements. SANS measurements were performed at three detector distances: 1, 4.5, and 13.5 m with a neutron wavelength of 6.0 Å. Sample run times were 5 min at 1 m, 15 min at 4.5 m, and 30 min at 13.5 m. The incoherent background scattering from the buffer solutions was subtracted from the SANS curves for each sample. SANS intensities are reported on an absolute scale in cm^{-1}. Error bars for SANS measurements represent standard error in the data when visible and are smaller than the plotting symbols when no error bars are visible.

Contrast matching for PEG/PAA IPNs was performed by preparing the IPNs with deuterated-PAA (d_4-PAA) in place of hydrogenated PAA. This allowed significant neutron scattering length density contrast between the PEG and d_4-PAA networks such that the two polymers could be independently contrast matched to the solvent by varying the ratio of D_2O to H_2O in the buffer solutions. The neutron scattering contrasts were obtained using the scattering length density calculator available from the NCNR Web site (http://www.ncnr.nist.gov/resources/).

Compressive Mechanical Testing. The initial compressive modulus, stress at break, and strain at break were determined using an Instron Universal Materials Testing Machine (Instron Model #5844) (Norwood, MA) with Bluehill 2 software. Compressive tests were performed on hydrogel cylinders 9 mm in diameter and 4 mm in height at a strain rate of 1 mm/min. The cylinders were obtained by cutting out 9 mm diameter cylinders with a trephine punch from a 4 mm thick hydrogel slab. Stress and strain are reported as true stress and true strain, assuming isotropic deformation during compression. Measurements for each type of sample were performed ten times. The initial compressive modulus was determined by taking the slope of the true stress/strain curve between 5 and 15% strain. The true strain at break was determined as the true strain reached before failure, which was indicated by a sudden drop in the true stress. The true stress at break was taken at maximum true strain before failure. Error bars for compressive mechanical measurements represent one standard deviation in the data.

In the previous work on PEG/PAA IPNs by Myung and co-workers, tensile stress−strain relationships were reported, but we focused on compressive stress−strain relationships in the current study.[16] This is because the compression testing method is far easier to perform and yields more consistent results than tensile measurements for the hydrogel samples. Tensile measurements are experimentally troublesome because it is difficult to prevent either the hydrogel from slipping out of the grips or the grips from damaging the hydrogel if clamped too tightly. Perhaps more significantly, the compression test method allows our work to be more directly comparable to the IPN work of Gong et al., wherein compression testing is used.

In general, the tensile measurements previously reported and the compressive mechanical properties reported here are similar; however, in some instances there are notable differences in the mechanical properties. These differences are not only representative of differences between tensile and compressive measurements but are also representative of differences between the synthesis methods used for the PEG-diacrylate macromonomers. The revised synthesis method for the PEG-diacrylate macromonomers used in this work led to PEG networks with higher moduli, lower strains at break, and lower equilibrium water contents than the PEG networks prepared by Myung and co-workers.

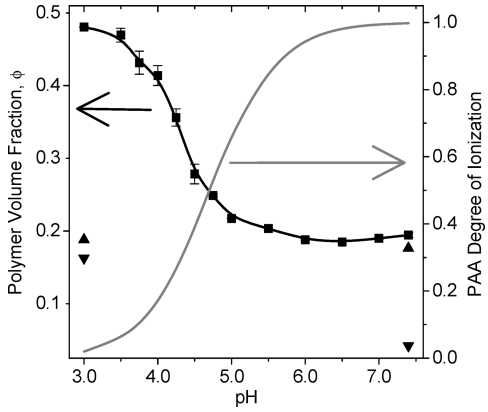

Figure 1. Polymer volume fraction (φ) as a function of pH for PEG(4.6K)/PAA IPN (■), PEG(4.6K) (▲), and PAA (▼) hydrogels. The gray curve shows the degree of PAA ionization (right axis) as a function of pH. The PEG/PAA IPNs were significantly less swollen than PEG or PAA single networks at pH 3.0 and had close to the same degree of swelling as PEG single networks at pH 7.4.

Table 1. Equilibrium Polymer Volume Fractions for PEG/PAA IPNs with Varying PEG M_n in pH 7.4 Buffer[a]

PEG M_n	polymer vol frac	PEG vol frac	PAA vol frac	vol ratio PAA:PEG
3.4K	0.23	0.06	0.17	2.8
4.6K	0.21	0.05	0.16	3.2
8.0K	0.12	0.02	0.10	4.4

[a] Standard deviations in the data are in the third decimal place.

RESULTS AND DISCUSSION

Swelling. Swelling measurements for PEG/PAA IPNs were performed as a function of pH. Figure 1 shows the equilibrium polymer volume fractions for a PEG(4.6K)/PAA hydrogel as a function of pH as well as the degree of ionization of the PAA carboxylic acid groups, which was calculated using a pK_a of 4.3. Increasing the PEG molecular weight in the IPNs shifted the polymer volume fraction versus pH curve down but did not change the general shape of the curve. Table 1 shows the composition of PEG/PAA IPNs with varying PEG molecular weight in terms of volume fractions of PEG, PAA, and overall polymer volume fractions at physiologically relevant pH 7.4.

At pH 3.0, PEG/PAA IPNs were not highly swollen and had a high polymer volume fraction compared to both PEG and PAA single networks. The high polymer volume fraction for PEG/PAA IPNs at low pH can be attributed to hydrogen-bonding complexation, which is known to occur between PEG and PAA.[22−28] Previous work in the literature has shown that there are three distinct pH regions that govern the complexation between PEG and PAA in solution.[28] At a pH well below the pK_a of acrylic acid (4.3), the two polymers form a hydrophobic interpolymer hydrogen-bonding complex that excludes water from interacting with both polymers. Over a narrow pH range bracketing the pK_a of acrylic acid (pH 4.0−4.75), the two

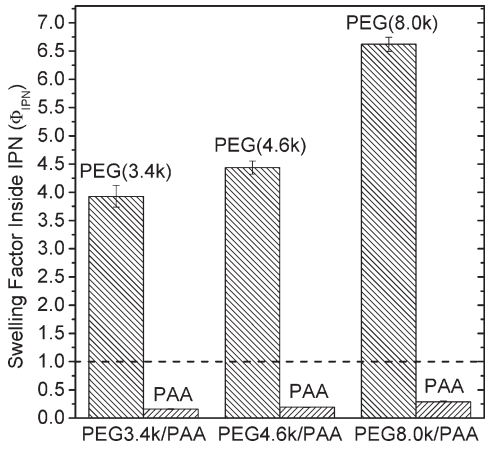

Figure 2. Volumetric swelling factors for PEG and PAA networks inside the IPN at pH 7.4 (Φ_{IPN}). A swelling factor of unity implies that the single network hydrogel is swollen to the same extent within the IPN as it is outside of the IPN. A swelling factor above unity implies that the single network hydrogel is swollen to a greater extent within the IPN, while a swelling factor below unity implies the converse.

polymers form a more hydrophilic complex as some of the carboxylic acid groups on the PAA ionize and begin to dissociate from the PEG network. Finally, at a pH well above the pK_a of acrylic acid, the two polymers no longer form an interpolymer complex and completely dissociate from one another. This description of the complexation between PEG and PAA is consistent with the swelling data for PEG/PAA IPNs (Figure 1). At low pH, there was a high polymer volume fraction due to the complexation between PEG and PAA. Near the pK_a of PAA, a transition occurred, and the PEG/PAA IPN hydrogel began to swell. Finally, at a pH well above the pK_a, where PEG and PAA are fully disassociated, the IPN hydrogel's swelling leveled off to a constant low polymer volume fraction.

At physiological pH 7.4, the swelling of the PEG/PAA IPN is driven primarily by the increased hydrophilicity of the ionized carboxylates and the osmotic swelling force induced by the ionized PAA network. The negative charges on the ionized carboxylate groups lead to a screened electrostatic repulsion between neighboring PAA chains. The buffer solutions used in this study had an ionic strength of 0.15 M, in which case the Debye length of the electrostatic interactions was ~0.8 nm, or about the length of two monomer units. Although long-range electrostatic interactions are not expected to be important at this ionic strength, the influx of counterions into the negatively charged hydrogel results in an additional large osmotic swelling force, which dramatically increases water uptake in order to balance the counterion concentration within the hydrogel. This generates what is known as a Donnan equilibrium between the gel and the surrounding solvent wherein both the electroneutrality condition and a balanced salt ion distribution within the gel and solution need to be achieved.[29]

In PEG/PAA IPNs, the osmotic swelling force is balanced by the elastic force required to stretch both the PEG and the PAA networks. At pH 7.4, the PEG network inside the IPN is forced to swell beyond its single network equilibrium swelling point, while the swelling of the PAA network inside the IPN is restricted by the elastic restoring force of the PEG network. Figure 2 represents the difference in swelling between PEG and PAA single network hydrogels inside the IPN and outside the IPN in terms of a volumetric swelling factor. The volumetric swelling factor (Φ_{IPN}) is defined in eq 1 as the ratio of an IPN hydrogel's equilibrium volume at pH 7.4 (V_{IPN}) to a single network hydrogel's equilibrium volume at pH 7.4 (V_{SN}) (prepared with the same initial volume as the IPN). A volumetric swelling factor of unity implies that the single network hydrogel at equilibrium swelling is swollen to the same extent within the IPN as it is outside the IPN.

$$\Phi_{IPN} = \frac{V_{IPN}}{V_{SN}} \quad (1)$$

The balance between the swelling of the PEG network and the PAA network is dependent upon the PEG molecular weight or the cross-link density of the PEG network. As the PEG molecular weight increases, the PEG network becomes less densely cross-linked and the PAA network is able to reach a swelling point closer to the equilibrium swelling point of a PAA single network. Although the PEG networks are stretched well beyond their initial single network swollen state, the overall polymer volume fraction for PEG/PAA IPNs at pH 7.4 is within 1−2% of the polymer volume fraction of the PEG single networks.

Small-Angle Scattering. Small-angle scattering was used to examine the molecular-level structural changes that occur when an end-linked PEG single network is interpenetrated with PAA and subsequently deformed by the osmotic swelling force induced by the ionized PAA network. In this study, SAXS and SANS provided complementary structural information. SAXS was used to probe differences in electron density, while SANS with contrast matching (selective deuteration) was used to probe the individual structures of both the PEG and PAA networks within the IPN hydrogel. The SAXS curves for a PEG(4.6K) single network, PAA single network, and PEG(4.6K)/PAA IPN are shown in Figure 3 for both pH 3.0 (a) and pH 7.4 (b). The SAXS curves demonstrate that there are clear structural differences between each of the three types of hydrogels.

PEG single networks have a distinct correlation peak near q = 0.5 nm^{-1}, which is not strongly affected by pH. PAA single networks have a single broad shoulder, which becomes shallower as the pH increases. PEG/PAA IPNs have broad shoulders in both the low-q (q < 1 nm^{-1}) and high-q (q > 1 nm^{-1}) regions, which become more pronounced as the pH increases. In the very high-q region (q > 5 nm^{-1}) all of the hydrogels show an upturn in the scattering intensity. This upturn is due to atomic scale interactions within the material. If the SAXS curves are not vertically shifted for clarity, then both the intensity and the shape of the SAXS curves in this region are very similar for each type of hydrogel.

The scattering and morphology of the PEG-diacrylate networks used in this study have been described in our previous work.[18] Briefly, the correlation peak indicates that these hydrogels have a weakly ordered structure. This weakly ordered structure comes from the well-defined macromonomer molecular weight between cross-link junctions, which have high functionality, estimated to range from 75 to 150 end-groups per cross-link junction, depending upon molecular weight of the PEG macromonomer.[18] These functionality estimates are consistent with networks prepared via free radical reactions wherein high degrees of polymerization are readily obtained.[30] The high functionality results in cross-link junctions with "molecular bottle-brush" morphology consisting of many PEG chains originating from extended cross-link junction regions within the

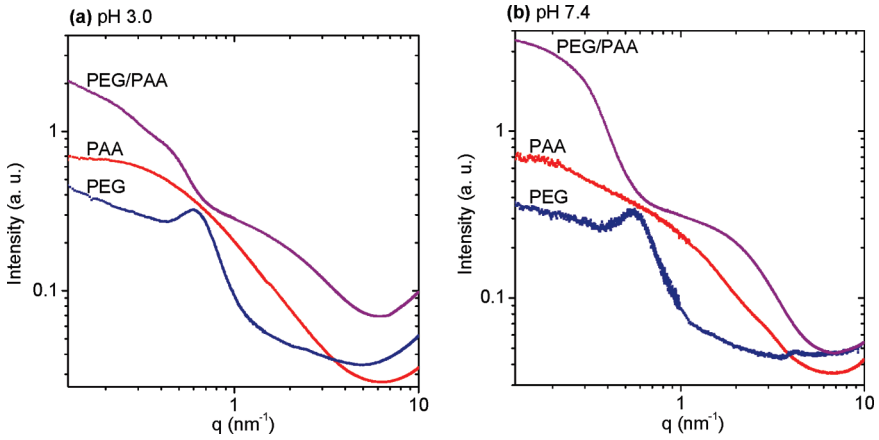

Figure 3. SAXS from a PEG(4.6K) single network (bottom curve), a PAA single network (middle curve), and a PEG(4.6K)/PAA IPN (top curve) at pH 3.0 (a) and pH 7.4 (b). PEG single networks have a correlation peak related to the cross-link spacing that is not strongly affected by pH. PAA single networks have a broad shoulder that becomes shallower as the pH increases. The scattering from PEG/PAA IPNs is strongly affected by pH, with broad shoulders forming in both the low-q (<1 nm^{-1}) and high-q (>1 nm^{-1}) regions at pH 7.4. Intensities are in arbitrary units (au) and have been offset for clarity.

polymer network. This morphology forms due to the steric hindrance of neighboring PEG chains, which forces the cross-link junctions to adopt a highly extended conformation.[31] The conformation of the polymer chains originating from the cross-link junctions have been modeled as either three-dimensional self-avoiding random walks or in some instances as more highly extended two-dimensional self-avoiding random walks.[32−34]

The average spacing between these cross-link junctions can be obtained from the correlation peak position by using Bragg's law (eq 2), where λ is the wavelength, q_{max} is the value of the scattering vector at the correlation peak maximum, d is the spacing between scattering centers, and θ is half of the scattering angle.

$$d = \frac{\lambda}{2\ sin\ \theta} = \frac{2\pi}{q_{max}} \qquad (2)$$

The cross-link junction spacing ranged between 6 and 16 nm, depending upon both the polymer volume fraction and the PEG molecular weight. PEG networks with a lower polymer volume fraction and/or a higher PEG molecular weight had a larger spacing between cross-link junctions.

It is clear from Figure 3 that the scattering pattern for PAA single networks is significantly different than for the end-linked PEG networks. The scattering from PAA networks consists of a single broad shoulder. This scattering pattern is typical for polymer solutions and randomly cross-linked hydrogels.[35] The broad shoulder can be fit to the generic Lorentzian model (eq 3):

$$I(q) = \frac{C}{1 + (\xi q)^m} + B \qquad (3)$$

where I is intensity, q is the scattering vector, ξ is the correlation length, m is the Porod exponent or fractal dimension of the scattering object, and C and B are q-independent fitting constants that depend only on the magnitude of the X-ray intensity (reported in arbitrary units). For semidilute polymer solutions and networks swollen in a good solvent, the correlation length, ξ, roughly translates to the average interchain polymer spacing.[35] The Porod exponent yields the fractal dimension of the scattering object, which is related to the polymer chain conformation and is essentially the inverse of the scaling exponent, ν. For a

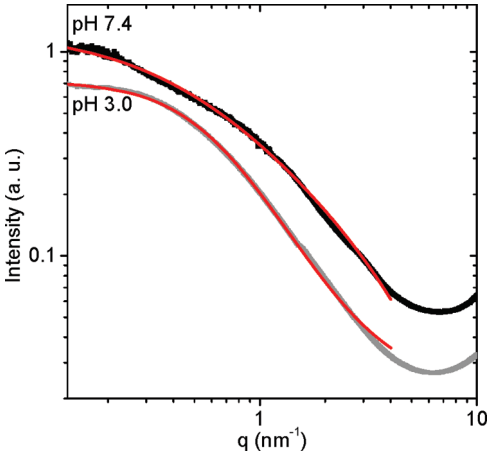

Figure 4. SAXS from PAA single networks at pH 7.4 (top) and pH 3.0 (bottom). The solid red curve shows a fit to a generic Lorentzian model (eq 3).

polymer chain modeled as a random walk or an ideal Gaussian chain, the scaling exponent is $\nu = 0.5$, yielding a fractal dimension, $d_f = 2$. Polymer chains that are more highly swollen are modeled better as self-avoiding random walks, where $\nu = 0.588$, yielding a fractal dimension, $d_f = 1.7$.[36] Figure 4 shows the scattering from a PAA single network at both pH 3.0 and pH 7.4 with fits to eq 3. As the pH was increased, the broad shoulder shifted to a lower q and the slope of the scattering curve flattened out. From fits to eq 3, the correlation length and fractal dimension shifted from $\xi = 1.6$ nm and $d_f = 2.1$ at pH 3.0 to $\xi = 2.1$ nm and $d_f = 1.2$ at pH 7.4. This is consistent with a more highly swollen PAA network at pH 7.4. At low pH, the value of the fractal dimension suggests that the PAA chains are modeled well as Gaussian chains, while at higher pH the chains become more fully extended when the network is more highly swollen.

PEG/PAA IPNs exhibited distinct structural transitions in response to pH. Figure 5 shows how the scattering curves changed as a function of pH near the pK_a of acrylic acid. At pH 3.0, PEG/PAA IPNs have a small structural feature near q = 0.5 nm^{-1} and a broader shoulder in the higher q region. As the

dx.doi.org/10.1021/ma200693e |*Macromolecules* 2011, 44, 5776–5787

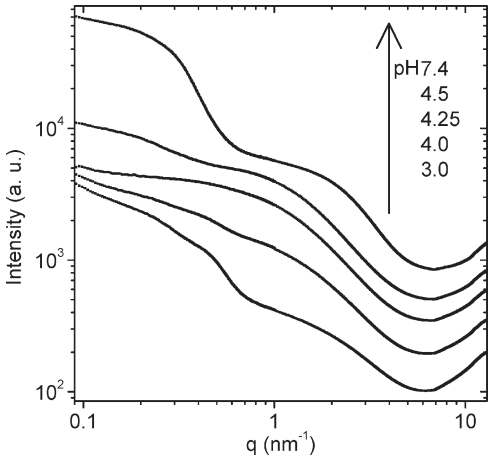

Figure 5. SAXS from a PEG(4.6K)/PAA IPN as a function of pH (pH increases from bottom to top curves). At pH 4.25 (middle curve), a transition occurred in the scattering as broad peaks began to develop in both the low-q, <1 nm^{-1}, and high-q, >1 nm^{-1}, regions. These transitions coincide with a dramatic increase in swelling above the pK_a of acrylic acid. Intensities are in arbitrary units (au) and have been offset for clarity.

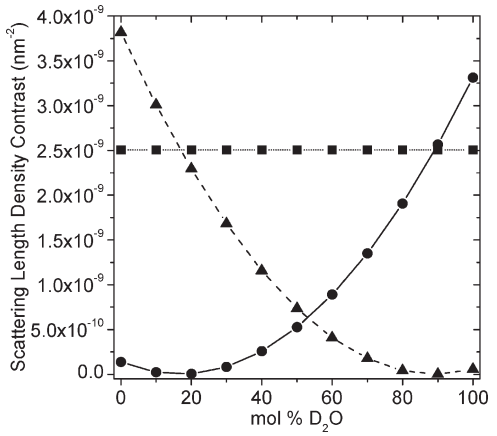

Figure 6. Neutron scattering length density contrast as a function of D_2O content for d_4-PAA: H_2O/D_2O (▲), PEG: H_2O/D_2O (●), and PEG: d_4-PAA (■). Contrast matching was used to isolate the scattering from solely the PEG network within the IPN (89 mol % D_2O) and solely the d_4-PAA network within the IPN (17 mol % D_2O). The neutron scattering contrasts were obtained using the resources available from the NCNR Web site (http://www.ncnr.nist.gov/resources/).

pH increased, the feature near $q = 0.5$ nm^{-1} first flattened out and then a broader shoulder developed in the low-q region. At the same time, the shoulder in the high-q region became more pronounced. Although SAXS is a useful probe of the electron density differences in IPN hydrogels, it is unable to distinguish between the individual structures of the PEG and PAA networks. Thus, in order to properly interpret the SAXS results, SANS with contrast matching was used to probe the structure of each individual component within the IPN.

SANS measurements were performed on PEG networks interpenetrated with d_4-PAA at both pH 3.0 and pH 7.4. In order to contrast-match out each individual network within the IPN, the IPN hydrogels were swollen in buffers with the appropriate ratios of D_2O to H_2O. Figure 6 shows the theoretical

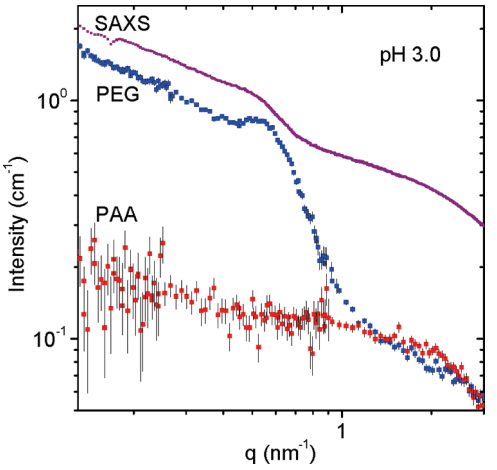

Figure 7. SAXS from a PEG(4.6K)/PAA IPN at pH 3.0 (top). SANS from a PEG(4.6K)/PAA IPN with contrast-matching conditions to reveal the PEG network inside the IPN at pH 3.0 (89 mol % D_2O) (middle) and contrast-matching conditions to reveal the PAA network inside the IPN at pH 3.0 (17 mol % D_2O) (bottom). The SANS curves reveal that the PEG network maintains a correlation peak related to the cross-link spacing when it is interpenetrated with PAA. The PAA network within the IPN has a featureless scattering curve, indicating a relatively homogeneous structure. The SAXS curve intensity has been offset for clarity.

scattering length density contrast (square of difference in scattering length densities) for PEG and d_4-PAA in terms of mol % D_2O in the buffer solution. From this figure, at 17 mol % D_2O, the PEG network has been contrast-matched to the solvent such that the scattering from a PEG/d_4-PAA IPN swollen in this buffer reveals primarily the PAA network within the IPN. Similarly, at 89 mol % D_2O, the scattering from the d_4-PAA network has been contrast-matched, revealing the scattering from the PEG network within the IPN.

Figure 7 shows the SAXS curve from a PEG/PAA IPN at pH 3.0 along with the SANS results at pH 3.0 with contrast-matching conditions for both the PEG and PAA networks. The SANS curves show that the PEG network within the IPN at pH 3.0 maintains a correlation peak in its scattering pattern. This indicates that the weakly ordered structure of the PEG network was not disrupted as a result of formation of the interpenetrating PAA network. The structure of the PEG network within the IPN at low pH is therefore very similar to the structure of a PEG single network. The scattering from the PAA network is weak at pH 3.0 and has no discernible features. This suggests that the cross-linked PAA network has a uniform structure with randomly oriented polymer chains.

The SAXS and SANS results at pH 7.4 are shown in Figure 8. The SANS results show that the broad shoulder at low q is much more intense when the SANS probes the structure of the PEG network. The inset in Figure 8 shows that the maximum SANS intensity of the low-q broad shoulder increases with increasing D_2O content, which is the same trend as calculated for the contrast-matching of the PEG network (Figure 6). These differences in SANS intensity as a function of D_2O content indicate that the low-q broad shoulder feature is generated by the PEG network. Although the low-q broad shoulder does not entirely disappear when the theoretical contrast-matching conditions for the PEG network are met (PAA curve in Figure 8), the residual intensity may be due to contrast between the PEG and

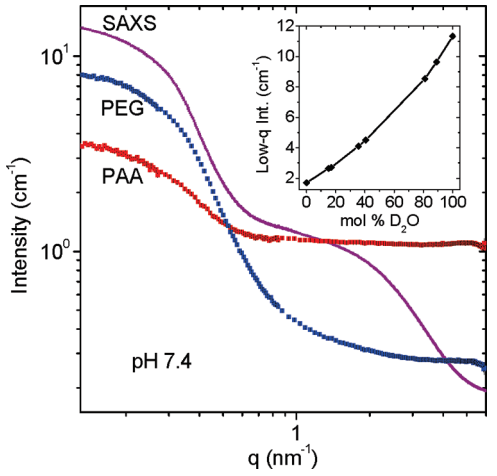

Figure 8. SAXS from a PEG(4.6K)/PAA IPN at pH 7.4 (top). SANS from a PEG(4.6K)/PAA IPN with contrast-matching conditions to reveal the PEG network inside the IPN at pH 7.4 (89 mol % D_2O) (middle) and contrast-matching conditions to reveal the PAA network inside the IPN at pH 7.4 (17 mol % D_2O) (bottom). The inset shows the maximum SANS intensity of the low-q broad shoulder as a function of D_2O content. The SANS shows that the intensity of the low-q broad shoulder is significantly higher when the contrast-match conditions to reveal the PEG network are met. The broad shoulder in the high-q region is not visible in SANS due to the large incoherent background scattering from hydrogenated species. The SAXS curve intensity has been offset for clarity.

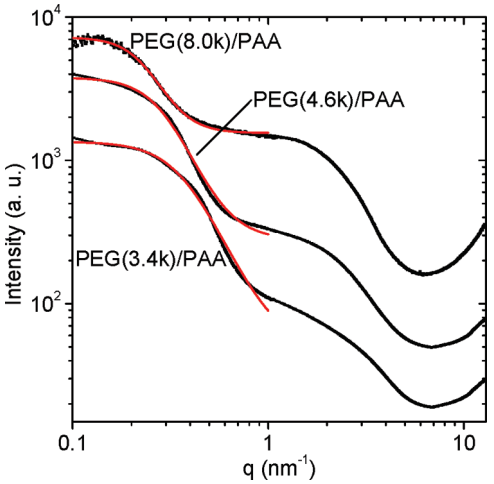

Figure 9. SAXS from PEG/PAA IPNs with PEG M_n = 8.0K (top), M_n = 4.6K (middle), and M_n = 3.4K (bottom). The location of the broad low-q feature shifts to a lower q (larger length scale) when the PEG M_n is increased. The solid red curve shows a fit of the low-q feature to a generic Lorentzian model (eq 3). The high-q broad feature becomes more pronounced with increasing PEG M_n and decreasing polymer volume fraction. This corresponds with a higher degree of hydration around the PAA network.

d_4-PAA networks within the IPN, which is independent of D_2O content (Figure 6).

The high-q broad shoulder in the scattering curves from PEG/PAA IPN hydrogels could not be resolved from SANS measurements since features on such small length scales were obscured by the incoherent background scattering from hydrogenated species within the samples. Fitting the high-q broad shoulder in the SAXS curve to the generic Lorentzian model (eq 3) yielded a correlation length of 0.4 nm independent of the PEG molecular weight. Since the high-q shoulder probes such a small length scale, the most reasonable explanation is that this feature is generated by the scattering cross-section of the hydrated PAA chains, wherein there is contrast between the polymer chain and the surrounding buffer. The high-q broad shoulder becomes more pronounced for IPN hydrogels that have a higher PEG molecular weight because these IPNs are more highly swollen and therefore the PAA chains have a higher degree of hydration (Figure 9).

In order to properly interpret the low-q broad shoulder scattering feature, it is important to consider the large degree of swelling that occurs when a PEG/PAA IPN is brought from pH 3.0 to pH 7.4. At pH 3.0, the PAA carboxylic acid moieties form hydrogen bonds with ether oxygens in the PEG backbone and the structure of the PEG network within the IPN is similar to the structure of a PEG single network. As the pH increases to near the pK_a of acrylic acid, the PAA network starts to become deprotonated but does not yet completely dissociate from the PEG network. The IPN hydrogel begins to swell and the PEG network is disrupted in a nonuniform manner that destroys the PEG network's weakly ordered structure, as indicated by a loss of the correlation peak in the small-angle scattering. At the pK_a of PAA, the SAXS curve flattens out in the low-q region, indicating that there are no longer any discernible structural features near this length scale (Figure 5). This occurs because the PEG network's weak order has been disrupted, but the PAA has not yet completely dissociated from the PEG network for there to be a distinct spatial separation between the two polymer networks. As the pH increases above the pK_a, the PAA completely dissociates from the PEG network resulting in a nanoscale separation between the two polymers. This coincides with the formation of the broad shoulder in the low-q region of the scattering curves. The spatial inhomogeneity between the PEG and PAA networks is on the nanoscale due to the physical constraints of the interpenetrating network. Limiting this spatial inhomogeneity to a length scale below the wavelength of visible light is highly desirable if optically clear hydrogels are required.

Since the low-q broad shoulder is generated by the PEG network, this scattering feature is attributed to scattering from nanoscale regions within the IPN that have a higher density of PEG chains. These regions consist of the high functionality cross-link junctions with "molecular bottle-brush" morphology. The low-q broad shoulder can be fit to a generic Lorentzian model (eq 3) to obtain the average size of the PEG-rich domains within the IPN. In Figure 9 it is observed that the position of the low-q broad shoulder shifts to a lower q or a larger length scale as the molecular weight of the PEG network increases. Fitting the Lorentzian model to the low-q broad shoulder (solid red curves in Figure 9), the size of the domains is ξ = 2.6 nm for PEG(3.4K)/PAA, ξ = 3.4 nm for PEG(4.6K)/PAA, and ξ = 4.4 nm for PEG(8.0K)/PAA. Interestingly, these domains sizes correspond well with the calculated radii of gyration for PEG chains modeled as three-dimensional self-avoiding random walks using a Kuhn length of 0.76 nm and a scaling exponent of ν = 0.588. These radii of gyration are calculated as 2.6 nm for PEG3.4K, 3.1 nm for PEG4.6K, and 4.3 nm for PEG8.0K. Although reasonable values are obtained for the correlation length, the limited q range of the broad shoulder cannot yield reliable values for the slope or the fractal dimension of the scattering object.

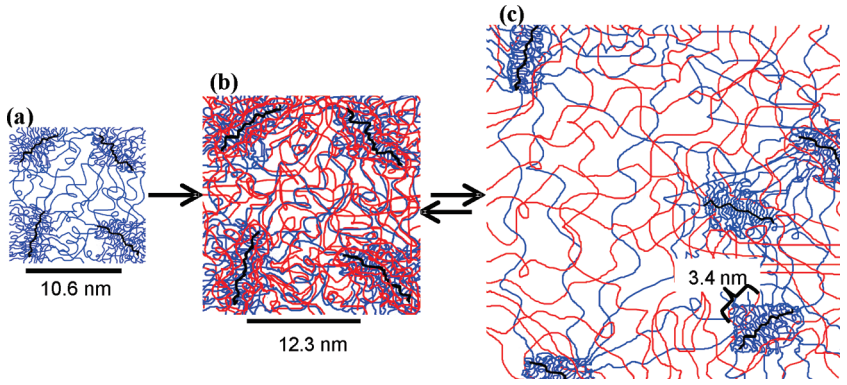

Figure 10. (a) Schematic depicting the structure of a PEG(4.6K) network with weakly ordered high functionality molecular bottle-brush cross-link junctions. (b) Schematic of a PEG(4.6K)/PAA IPN at low pH where the PAA complexes with the PEG network, which maintains its weak ordering. (c) Schematic of PEG(4.6K)/PAA IPN at high pH with highly extended PEG chains and disordered regions of higher PEG chain density surrounding the molecular bottle-brush cross-link junctions. The size of each schematic is shown roughly to scale to give an indication of the volume increase in each step.

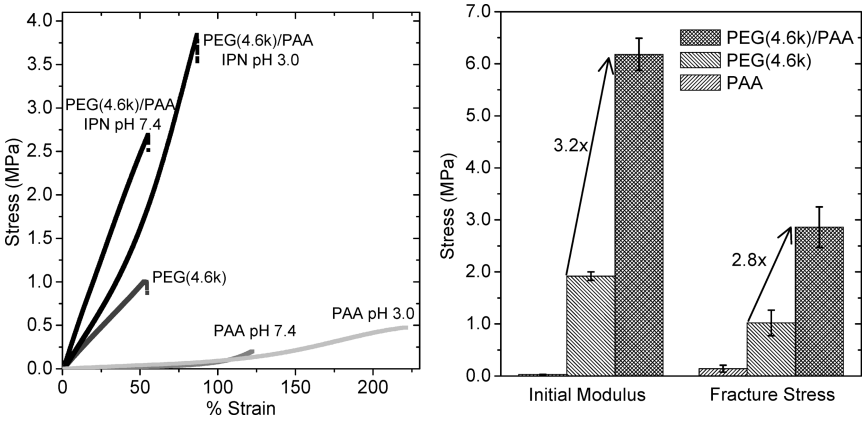

Figure 11. (a) Stress−strain behavior for a PEG(4.6K)/PAA IPN, PEG(4.6K), and PAA hydrogel at pH 3.0 and pH 7.4. (b) Initial modulus and stress at break for a PEG(4.6K)/PAA IPN, PEG(4.6K), and PAA hydrogel at pH 7.4. The initial modulus and fracture strength of a PEG(4.6K)/PAA IPN hydrogel at pH 7.4 is 3-fold that of a PEG(4.6K) single network.

Figure 10 shows a summary schematic depicting the structure of a PEG single network, a PEG/PAA IPN at pH 3.0, and a PEG/PAA IPN at pH 7.4 as determined by the scattering results. The size of each hydrogel schematic is shown roughly to scale for a PEG(4.6K) network. This gives an indication of the volume increase that occurs as a PEG single network is interpenetrated with PAA and brought to pH 7.4.

The PEG single networks have cross-link junctions with high functionality and "molecular bottle-brush" morphology. For PEG/PAA IPNs at low pH, the PAA forms a hydrogen-bonding complex with the PEG and the weakly ordered structure of the PEG network is maintained. As the pH is increased to physiological pH 7.4, the carboxylic acid groups on the PAA become deprotonated and dissociate from the PEG chains. However, the PAA cannot dissociate on a large length scale due to the constraints of the IPN. This results in a nanoscale spatial separation between the PEG-rich high functionality cross-link junctions and the PAA network within the IPN. The osmotic swelling force of the PAA network forces the PEG network to swell and disrupts its weak ordering such that the PEG domains are not ordered enough for a correlation peak to be present. The transition from the structure at pH 3.0 to pH 7.4 is reversible from the perspective of small-angle scattering as there is no discernible difference between the scattering from IPNs that were never at high pH compared to the IPNs that were brought to high pH and subsequently returned to low pH (Figure S01, Supporting Information). However, for PEG/PAA IPNs greater than 2 mm in thickness, the process of rapidly exchanging buffers from pH 7.4 to pH 3.0 results in visible macroscopic crack formation within the hydrogels, which leads to a reduction in the initial modulus as well as the stress and strain at break.

Compressive Mechanical Testing. As outlined in the previous sections, PEG single networks, PAA single networks, and PEG/PAA IPNs each have distinct molecular-level structures and swelling properties. It should not be surprising, then, that the compressive mechanical properties for each type of hydrogel are notably different. Figure 11a shows typical compressive stress−strain curves for a PEG(4.6K) single network, a PAA single network, and a PEG(4.6K)/PAA IPN at both pH 3.0 and pH 7.4. Figure 11b shows a summary of the initial moduli and fracture stresses for each type of hydrogel at pH 7.4. The loosely cross-linked PAA single networks had a high strain at break; however, the low cross-linking density and polymer volume fraction yielded hydrogels with very low initial moduli and fracture stresses in comparison to both PEG(4.6K) single networks and PEG(4.6K)/PAA IPNs. At pH 3.0, PEG(4.6K)/PAA IPNs had a

dx.doi.org/10.1021/ma200693e |*Macromolecules* 2011, 44, 5776–5787

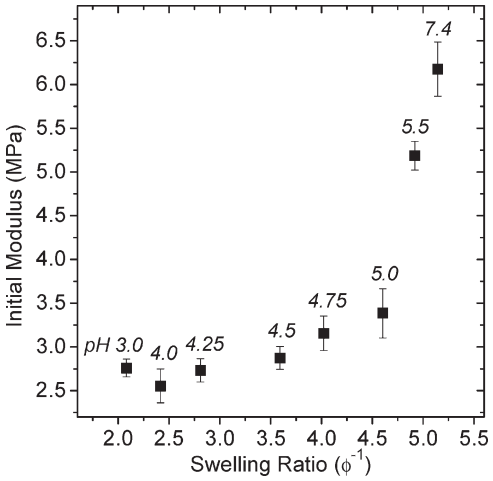

Figure 12. Initial modulus of a PEG(4.6K)/PAA IPN hydrogel versus the swelling ratio or the inverse of the polymer volume fraction (φ^{-1}). The swelling ratio of the IPN was controlled by changing the pH. As the pH increased, the IPN became more highly swollen and the initial modulus increased significantly.

high polymer volume fraction (φ = 0.48) compared to PEG(4.6K) single networks (φ = 0.22). Given the high polymer volume fraction and the increased cross-link density, it is reasonable that the initial modulus and the fracture strength of PEG(4.6K)/PAA IPNs at low pH increased significantly compared to PEG single networks. However, the interesting aspect of PEG/PAA IPNs is that as the pH was raised and the polymer volume fraction decreased substantially (decreased number of elastically effective chains per unit volume), the modulus of these networks continued to increase rather than decrease.

Figure 12 shows the initial modulus of PEG(4.6K)/PAA IPNs as a function of the hydrogel swelling ratio, which is the inverse of the polymer volume fraction (φ). IPNs with different equilibrium swelling ratios were obtained by controlling the pH (Figure 1). As the swelling ratio increased, the initial modulus of the IPNs gradually increased at lower swelling ratios but then increased dramatically at higher swelling ratios when the pH was above 5.0. Although PEG(4.6K)/PAA IPN hydrogels and PEG single network hydrogels had similar swelling ratios (Figure 1), the PEG(4.6K)/PAA IPNs at pH 7.4 had roughly a 3-fold increase in both initial modulus and fracture strength compared to PEG(4.6K) single networks. Similar trends were observed for PEG/PAA IPNs with PEG M_n = 3.4K and 8.0K, with higher modulus values observed for lower molecular weight PEG macromonomers.

To understand the enhancement in mechanical properties that occurs when a PEG single network is interpenetrated with PAA and subsequently swollen in pH 7.4 buffer, it is important to consider the swelling and structural transitions that occur during this process. According to the classical Flory–Rehner affine model treatment[29] and more recent scaling-based models developed by Urayama,[37] the equilibrium swelling ratio and the initial modulus of a swollen polymer network may be determined from a balance of the elastic free energy required to stretch a network chain and the free energy of mixing or the osmotic swelling force of the polymer chains in solution. The swelling of the polymer network is driven by the entropically favorable free energy of mixing for the polymer chains with solvent but resisted by the entropic penalty paid for stretching the network chains. The equilibrium swelling ratio of the polymer network is determined when the total free energy is minimized through a balance of these two opposing forces. For a network that includes an ionized polymer such as PAA at high pH, additional electrostatic repulsive and osmotic swelling forces from counterions in solution also contribute significantly to the equilibrium swelling ratio and consequently to the initial modulus of the swollen network.

For a PEG/PAA IPN, as the pH increases, the electrostatic repulsive and additional osmotic swelling force increase significantly as a result of PAA ionization, which drives the IPN to reach a higher equilibrium swelling ratio. Essentially, the PEG network is forced to expand well beyond its initial equilibrium swelling point by the osmotic swelling force of the second PAA network. This results in PEG chains within the IPN that are in a highly extended, non-Gaussian conformation.

Previous work has shown both theoretically and experimentally that the finite extensibility of highly extended polymer chains leads to an increase in the modulus of polymer networks due to the large entropic penalty for stretching a network chain to near full extension.[36,38−42] Theoretical models for force versus chain extension such as the inverse Langevin and the wormlike chain model predict a significant increase in the force required to stretch a polymer chain as it reaches its maximum extensibility.[36,38] Experimentally, Mark and co-workers showed that polydimethylsiloxane (PDMS) networks at high extension have an increased modulus due to the effects of finite chain extensibility.[39−42]

Small-angle scattering measurements along with swelling measurements give a quantitative measure of the PEG chain extension during the transition from a PEG single network to a fully swollen PEG/PAA IPN at pH 7.4. Since the PEG networks are end-linked, the average spacing between cross-link junctions can be assumed to be the average end-to-end distance of the PEG chains within the network. When a PEG(4.6K) network is first formed at a concentration of 50% w/w (polymer volume fraction, φ = 0.48), the measured cross-link spacing obtained from the correlation peak position using eq 2 is 7.2 nm, which is close to the end-to-end distance predicted for a PEG(4.6K) chain modeled as a three-dimensional self-avoiding random walk (7.6 nm). After the PEG(4.6K) network is allowed to swell to equilibrium (φ = 0.22), the cross-link spacing increases to 10.6 nm. The PEG(4.6K) network is then interpenetrated with PAA at low pH (φ = 0.48), at which point the PEG(4.6K) network maintains its structure and expands beyond its equilibrium swelling point to 12.3 nm at pH 3.0. As the pH increases to pH 7.4, the PEG(4.6K)/PAA IPN swells substantially (φ = 0.21) and the short-range ordering of the PEG(4.6K) network is lost. Although the end-to-end distance of the PEG chains within the network can no longer be measured from a correlation peak position, the average end-to-end distance can be estimated by measuring the macroscopic volumetric swelling increase and assuming affine deformation of the network chains. Using this assumption, the average end-to-end distance of the PEG(4.6K) chains within a PEG(4.6K)/PAA IPN at pH 7.4 is 17.3 nm. Similar calculations were performed for IPNs prepared with PEG(3.4K) and PEG(8.0K) macromonomers (Table 2).

To put the end-to-end distance of the PEG chains into context, Table 2 reports the average measured end-to-end distances of the PEG chains inside a single network (r_{SN}) and inside an IPN (r_{IPN}) divided by the contour length of a fully extended the PEG chain (r_{max}). For a PEG/PAA IPN at pH 7.4, the average PEG

Table 2. Cross-Link Spacing (PEG Chain End-to-End Distances) Compared to the PEG Chain Contour Length[a]

PEG M_n	PEG SN (r_{SN}) (nm)	vol expansion SN to IPN	projected IPN (r_{IPN}) (nm)	contour length (r_{max}) (nm)	r_{SN}/r_{max}	r_{IPN}/r_{max}
3.4K	8.5	1.58	13.4	28.0	0.30	0.48
4.6K	10.6	1.64	17.3	37.9	0.28	0.46
8.0K	15.7	1.88	29.5	65.9	0.24	0.45

[a] End-to-end distances were obtained from SAXS for PEG single networks (SN) and were projected for PEG/PAA IPNs assuming affine swelling.

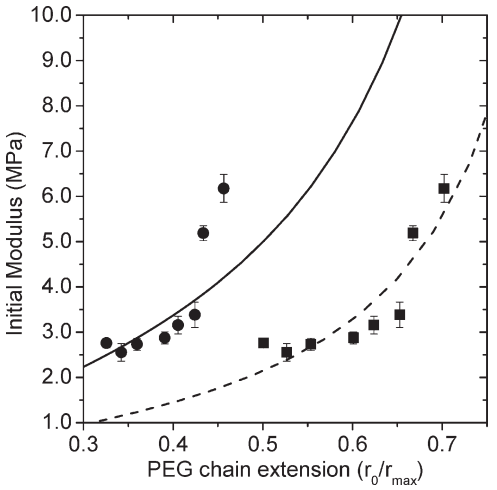

Figure 13. Initial moduli of PEG(4.6K)/PAA IPN hydrogel versus the PEG chain extension ratio within the IPN. Circular data points (●) represent the PEG chain extension ratio using the contour length as the maximum achievable extension while the square data points (■) represent the extension ratio calculated using 65% of the contour length. The solid and dashed curves represent best fits to the wormlike chain model for the force versus chain extension for a single polymer chain.

chain extension ratio does not significantly depend on the PEG molecular weight and is r_{IPN}/r_{max} = 0.45−0.48. It should be noted that these values are estimated averages since it is known from the scattering data that the PEG network within the IPN at pH 7.4 no longer has a weakly ordered structure. This implies that some PEG chains are extended beyond this extension ratio, while other PEG chains within the network are not as highly extended.

Previous work by Mark and co-workers on PDMS networks has shown that increases in modulus due to finite chain extensibility occur at extension ratios as low as r_0/r_{max} = 0.49−0.65.[39,41] Although the PEG chain extension ratios measured here are toward the lower end of the range for effects due to finite chain extensibility to become significant, the maximum extension of a PEG chain inside of an IPN may be significantly lower than the theoretically calculated contour length. Physical entanglements within the IPN act as constraining points for the PEG chains, which reduce the value of r_{max} and effectively increase the extension ratio of the PEG chains within the IPN. In fact, previous work in the literature has shown that entanglements reduce the effective molecular weight between cross-links such that the effects of finite extensibility become significant at lower extension ratios than would otherwise be expected for an unentangled polymer chain.[43]

To illustrate the effect of a reduced maximum PEG chain extension, Figure 13 plots the modulus of PEG(4.6K)/PAA IPNs versus the PEG chain extension ratio calculated using both the contour length (●) and 65% of the contour length value (■) for r_{max}. The solid and dashed lines represent fits to an approximate analytic expression of the wormlike chain model for the force versus chain extension of a single polymer chain. The analytic expression for the wormlike chain model is shown in eq 4

$$f \cong A\frac{kT}{b}\left(\frac{2r_0}{r_{max}} + \frac{1}{2}\left(\frac{r_{max}}{r_{max} - r_0}\right) - \frac{1}{2}\right) \qquad (4)$$

where f is the force, k is the Boltzmann constant, T is the temperature, b is the Kuhn length (0.76 nm), r_{max} is the end-to-end distance at full chain extension, r_0 is the actual end-to-end distance, and A is an arbitrary scaling factor used as a fitting parameter.[36,44] Since this model was derived for a single polymer chain, an arbitrary factor, A, was added such that the magnitude of the force could match that of the IPN. Using the factors r_{max} and A as fitting parameters, the best fit to this model is obtained when r_{max} = 24.4 nm or 65% of the true contour length of the PEG macromonomer. Although it is recognized that this model was derived for a single polymer chain and not a swollen IPN, its use here is merely to illustrate the extent to which the force required to strain a polymer chain is affected by finite extensibility. More elaborate models for the modulus of entangled networks have been developed by Edwards and Vilgis;[43] however, these models contain a number fitting parameters that may not be readily determined or may not make intuitive sense for an IPN network. For these reasons, eq 4 is used here for simplicity in order to show that the PEG chains within the IPN have extension ratios in the range where the effects of finite chain extensibility become significant. Given that the values for the PEG chain extension ratio are near the range where a substantial increase in modulus is expected, the finite extensibility of the PEG chains largely explains why an enhancement in modulus occurs as a PEG single network is converted to a PEG/PAA IPN and brought to pH 7.4.

In addition to the finite extensibility of the PEG chains, physical entanglements within the IPN, which act as additional cross-link points, also contribute to the modulus. Although these physical entanglements certainly contribute to the overall modulus, it is not expected that they are directly responsible for the increase in modulus that occurs as the IPN swells in response to pH. An increase in the modulus as the hydrogel becomes more highly swollen is more consistent with the effects of finite chain extensibility than the effects of physical entanglements.

While still based on an interpenetrating polymer network design, our high modulus PEG/PAA IPN hydrogels have a considerably different molecular level structure and mechanism for strength enhancement than the high-tear-strength "double-network" IPN hydrogels developed by Gong and co-workers.[1] In both systems, key similarities are (i) one network is tightly cross-linked while the other network is loosely cross-linked, (ii) one network is neutral while the other network is ionized, and (iii) the two networks have favorable interactions with each other. The key difference between these two systems is essentially the order of incorporation of the neutral and ionized networks within

dx.doi.org/10.1021/ma200693e |Macromolecules 2011, 44, 5776–5787

the IPN or in which network the highest degree of swelling occurs. For the high-tear-strength hydrogels prepared by Gong and co-workers, the first network is a highly swollen ionized network that is subsequently interpenetrated with a loosely cross-linked neutral network. The second network essentially acts to suppress crack propagation from cracks that form in the first tightly cross-linked network. For PEG/PAA IPNs, the first network is a tightly cross-linked neutral network that is interpenetrated with a loosely cross-linked ionized network. A substantial degree of swelling occurs after formation of the second network, resulting in a highly extended first network. The finite extensibility of the polymer chains in the tightly cross-linked first network results in an enhancement in modulus and fracture strength rather than an enhancement in tear strength.

CONCLUSIONS

Hydrogels with enhanced modulus and fracture strength are obtained by interpenetrating a tightly cross-linked PEG network with a loosely cross-linked PAA network. At low pH, the PAA forms a hydrogen-bonding complex with the PEG. As the pH is increased, the PAA dissociates from the PEG network and induces an osmotic swelling force. Small-angle scattering combined with swelling measurements give insight into the molecular level structure of PEG/PAA IPNs and the average extension of the PEG chains within the IPN. The swelling induced by the ionization of PAA disrupts the short-range ordering of the PEG network, forces the PEG chains to adopt highly extended conformations, and results in nanoscale spatial separation between the two polymers. The modulus of PEG/PAA IPN hydrogels is enhanced due to the non-Gaussian conformation and the finite extensibility of the PEG network chains within the first tightly cross-linked network.

The design principles that result in an enhanced modulus and fracture strength for PEG/PAA IPN hydrogels may be applied to other swollen polymer networks. The general principle is that a tightly cross-linked network is interpenetrated with a second network that subsequently swells in response to a controllable variable such as the pH. The swelling induced by the second network forces the polymer chains within the first network to become highly extended. This technique enhances the modulus of swollen polymer networks while maintaining a polymer volume fraction similar to the first network. This general design principle is different than for the "double-network" IPN hydrogels previously reported wherein a loosely cross-linked neutral network interpenetrates a highly swollen ionic network and tear strength is the primary attribute enhanced.

ASSOCIATED CONTENT

Supporting Information. Figure S01. This material is available free of charge via the Internet at http://pubs.acs.org.

AUTHOR INFORMATION

Corresponding Author

*Tel +1 650 723 4573; fax +1 650 723 9780; e-mail Curt.Frank@stanford.edu.

ACKNOWLEDGMENT

The authors acknowledge the National Institutes of Health (NIH) grant R01 EY016987-03 for funding. Portions of this research were carried out at the Stanford Synchrotron Radiation Lightsource (SSRL), a national user facility operated by Stanford University on behalf of the U.S. Department of Energy, Office of Basic Energy Sciences. The authors thank John Pople at SSRL for assistance with SAXS measurements on beamline 1-4 and Anne Martel and Thomas Weiss at SSRL for assistance with measurements on beamline 4-2. Dr. Jackson thanks NIST, U.S. Department of Commerce for support under cooperative agreement 70NANB7H6178. The authors thank Boualem Hammouda at the NIST Center for Neutron Research (NCNR) and Prof. Andrew Spakowitz at Stanford University for helpful discussions.

Certain commercial equipment, materials, suppliers and software are identified in this paper to foster understanding. Such identification does not imply recommendation or endorsement by the National Institute of Standards and Technology, nor does it imply that the materials or equipment identified are necessarily the best available for the purpose.

REFERENCES

(1) Gong, J. P.; Katsuyama, Y.; Kurokawa, T.; Osada, Y. *Adv. Mater.* **2003**, *15* (14), 1155–1158.

(2) Na, Y. H.; Kurokawa, T.; Katsuyama, Y.; Tsukeshiba, H.; Gong, J. P.; Osada, Y.; Okabe, S.; Karino, T.; Shibayama, M. *Macromolecules* **2004**, *37* (14), 5370–5374.

(3) Tanaka, Y.; Kuwabara, R.; Na, Y. H.; Kurokawa, T.; Gong, J. P.; Osada, Y. *J. Phys. Chem. B* **2005**, *109* (23), 11559–11562.

(4) Tsukeshiba, H.; Huang, M.; Na, Y. H.; Kurokawa, T.; Kuwabara, R.; Tanaka, Y.; Furukawa, H.; Osada, Y.; Gong, J. P. *J. Phys. Chem. B* **2005**, *109* (34), 16304–16309.

(5) Na, Y. H.; Tanaka, Y.; Kawauchi, Y.; Furukawa, H.; Sumiyoshi, T.; Gong, J. P.; Osada, Y. *Macromolecules* **2006**, *39* (14), 4641–4645.

(6) Huang, M.; Furukawa, H.; Tanaka, Y.; Nakajima, T.; Osada, Y.; Gong, J. P. *Macromolecules* **2007**, *40* (18), 6658–6664.

(7) Webber, R. E.; Creton, C.; Brown, H. R.; Gong, J. P. *Macromolecules* **2007**, *40* (8), 2919–2927.

(8) Tominaga, T.; Tirumala, V. R.; Lin, E. K.; Gong, J. P.; Furukawa, H.; Osada, Y.; Wu, W. L. *Polymer* **2007**, *48* (26), 7449–7454.

(9) Tirumala, V. R.; Tominaga, T.; Lee, S.; Butler, P. D.; Lin, E. K.; Gong, J. P.; Wu, W. L. *J. Phys. Chem. B* **2008**, *112* (27), 8024–8031.

(10) Furukawa, H.; Kuwabara, R.; Tanaka, Y.; Kurokawa, T.; Na, Y. H.; Osada, Y.; Gong, J. P. *Macromolecules* **2008**, *41* (19), 7173–7178.

(11) Tominaga, T.; Tirumala, V. R.; Lee, S.; Lin, E. K.; Gong, J. P.; Wu, W. L. *J. Phys. Chem. B* **2008**, *112* (13), 3903–3909.

(12) Nakajima, T.; Tanaka, Y.; Furukawa, H.; Kurokawa, T.; Gong, J. P. *Kobunshi Ronbunshu* **2008**, *65* (12), 707–715.

(13) Tanaka, Y.; Kawauchi, Y.; Kurokawa, T.; Furukawa, H.; Okajima, T.; Gong, J. P. *Macromol. Rapid Commun.* **2008**, *29* (18), 1514–1520.

(14) Yu, Q. M.; Tanaka, Y.; Furukawa, H.; Kurokawa, T.; Gong, J. P. *Macromolecules* **2009**, *42* (12), 3852–3855.

(15) Gong, J. P. *Soft Matter* **2010**, *6* (12), 2583–2590.

(16) Myung, D.; Koh, W. U.; Ko, J. M.; Hu, Y.; Carrasco, M.; Noolandi, J.; Ta, C. N.; Frank, C. W. *Polymer* **2007**, *48*, 5376–5387.

(17) Myung, D.; Waters, D.; Wiseman, M.; Duhamel, P. E.; Noolandi, J.; Ta, C. N.; Frank, C. W. *Polym. Adv. Technol.* **2008**, *19* (6), 647–657.

(18) Waters, D. J.; Engberg, K.; Parke-Houben, R.; Hartmann, L.; Ta, C. N.; Toney, M. F.; Frank, C. W. *Macromolecules* **2010**, *43* (16), 6861–6870.

(19) Elbert, D. L.; Hubbell, J. A. *Biomacromolecules* **2001**, *2* (2), 430–441.

(20) Welsh, W. J. *Physical Properties of Polymers Handbook*; AIP Press: Woodbury, NY, 1996.

(21) Arnold, R. *J. Colloid Sci.* **1957**, *12* (6), 549–556.

(22) Nishi, S.; Kotaka, T. *Macromolecules* **1985**, *18* (8), 1519–1525.

(23) Nishi, S.; Kotaka, T. *Macromolecules* **1986**, *19* (4), 978–984.

(24) Oyama, H. T.; Tang, W. T.; Frank, C. W. *Macromolecules* **1987**, *20* (3), 474–480.
(25) Iliopoulos, I.; Halary, J. L.; Audebert, R. *J. Polym. Sci., Part A: Polym. Chem.* **1988**, *26* (1), 275–284.
(26) Nishi, S.; Kotaka, T. *Polym. J.* **1989**, *21* (5), 393–402.
(27) Ilmain, F.; Tanaka, T.; Kokufuta, E. *Nature* **1991**, *349* (6308), 400–401.
(28) Khutoryanskiy, V. V.; Dubolazov, A. V.; Nurkeeva, Z. S.; Mun, G. A. *Langmuir* **2004**, *20* (9), 3785–3790.
(29) Flory, P. J. *Principles of Polymer Chemistry*; Cornell University Press: Ithaca, NY, 1953.
(30) Rikkou, M. D.; Patrickios, C. S. *Macromolecules* **2008**, *41* (16), 5957–5959.
(31) Wataoka, I.; Urakawa, H.; Kajiwara, K.; Schmidt, M.; Wintermantel, M. *Polym. Int.* **1997**, *44* (3), 365–370.
(32) Saariaho, M.; Szleifer, I.; Ikkala, O.; ten Brinke, G. *Macromol. Theory Simul.* **1998**, *7* (2), 211–216.
(33) Shiokawa, K.; Itoh, K.; Nemoto, N. *J. Chem. Phys.* **1999**, *111* (17), 8165–8173.
(34) Rathgeber, S.; Pakula, T.; Wilk, A.; Matyjaszewski, K.; Beers, K. L. *J. Chem. Phys.* **2005**, *122* (12), xxxx.
(35) Bastide, J.; Candau, S. J. Structure of Gels as Investigated by Means of Static Scattering Techniques. In *Physical Properties of Polymeric Gels*; Cohen, J. P., Ed.; John Wiley & Sons Ltd.: West Sussex, England, 1996; pp 143−308.
(36) Rubinstein, M.; Colby, R. H. *Polymer Physics*; Oxford University Press: New York, 2003; p 326.
(37) Urayama, K.; Kohjiya, S. *J. Chem. Phys.* **1996**, *104* (9), 3352–3359.
(38) Treloar, L. R. G. *The Physics of Rubber Elasticity*, 3rd ed.; Oxford University Press: London, 1975.
(39) Andrady, A. L.; Llorente, M. A.; Mark, J. E. *J. Chem. Phys.* **1980**, *72* (4), 2282–2290.
(40) Andrady, A. L.; Llorente, M. A.; Mark, J. E. *J. Chem. Phys.* **1980**, *73* (3), 1439–1445.
(41) Llorente, M. A.; Andrady, A. L.; Mark, J. E. *J. Polym. Sci., Part B: Polym. Phys.* **1981**, *19* (4), 621–630.
(42) Llorente, M. A.; Andrady, A. L.; Mark, J. E. *Colloid Polym. Sci.* **1981**, *259* (11), 1056–1061.
(43) Edwards, S. F.; Vilgis, T. *Polymer* **1986**, *27* (4), 483–492.
(44) Marko, J. F.; Siggia, E. D. *Macromolecules* **1995**, *28* (26), 8759–8770.